WARWICK
THE UNIVERSITY OF WARWICK

Manuscript version: Author's Accepted Manuscript
The version presented in WRAP is the author's accepted manuscript and may differ from the published version or Version of Record.

Persistent WRAP URL:
http://wrap.warwick.ac.uk/148200

How to cite:
Please refer to published version for the most recent bibliographic citation information. If a published version is known of, the repository item page linked to above, will contain details on accessing it.

Copyright and reuse:
The Warwick Research Archive Portal (WRAP) makes this work by researchers of the University of Warwick available open access under the following conditions.

Copyright © and all moral rights to the version of the paper presented here belong to the individual author(s) and/or other copyright owners. To the extent reasonable and practicable the material made available in WRAP has been checked for eligibility before being made available.

Copies of full items can be used for personal research or study, educational, or not-for-profit purposes without prior permission or charge. Provided that the authors, title and full bibliographic details are credited, a hyperlink and/or URL is given for the original metadata page and the content is not changed in any way.

Publisher's statement:
Please refer to the repository item page, publisher's statement section, for further information.

For more information, please contact the WRAP Team at: wrap@warwick.ac.uk.

warwick.ac.uk/lib-publications

Complete Manuscript

Effect of compression reduction on deformation of CaO-CaS-Al_2O_3-MgO inclusions in solid and semi-solid steel

Dr. Yi Wang
Lecturer at School of Metallurgical and Ecological Engineering, University of Science and Technology Beijing (USTB), Beijing 100083, China
Email: wangyi@metall.ustb.edu.cn

Prof. Lifeng Zhang (Correspondence Author)
Professor at State Key Laboratory of Metastable Materials Science and Technology, School of Mechanical Engineering, Yantian University, Qinhuangdao City, Hebei Province 066004, China
Email: zhanglifeng@ysu.edu.cn
Phone number: 86-0335-8074666

Prof. Ying Ren (Correspondence Author)
Professor at School of Metallurgical and Ecological Engineering, University of Science and Technology Beijing (USTB), Beijing 100083, China
Email: yingren@ustb.edu.cn

Dr. Zushu Li (Correspondence Author)
Reader at Advanced Steel Research Centre, WMG, University of Warwick, Coventry, CV4 7AL, U.K.
Email: z.li.19@warwick.ac.uk

Dr. Carl Slater
Research fellow at Advanced Steel Research Centre, WMG, University of Warwick, Coventry, CV4 7AL, U.K.
Email: c.d.slater@warwick.ac.uk

Mr. Kaiyu Peng
PhD. student at School of Metallurgical and Ecological Engineering, University of Science and Technology Beijing (USTB), Beijing 100083, China
Email: pengkaiyu_sgqg@163.com

Mr. Fenggang Liu
PhD. student at School of Metallurgical and Ecological Engineering, University of Science and Technology Beijing (USTB), Beijing 100083, China
Email: liufenggang_sgqg@163.com

Mr. Yanyu Zhao
PhD. student at School of Metallurgical and Ecological Engineering, University of Science and Technology Beijing (USTB), Beijing 100083, China
Email: zhaoyanyu_sgqg@163.com

Abstract:

Plain strain deformation was performed on solid steel samples at 1473 K and semi-solid steel at 1743 K. The deformation of inclusions under reductions of 10%, 20%, and 30% was studied. In solid steel deformed at 1473 K, the average aspect ratio of inclusions increased from 1.23 in the original slab to 2.07, 2.23, and 2.30 under the reduction of 10%, 20%, and 30%. The deformation of inclusions in semi-solid steel was hardly influenced by reduction. The deformation of inclusions was much more in solid steel than that in semi-solid steel in the current study. Inclusion deformation was determined by the difference of hardness between inclusion phase and steel matrix. Stress-strain curves during deformations indicated that semi-solid steel matrix at 1743 K was much softer than the solid steel matrix at 1473 K. Compared to the composition of inclusions in the original slab, the CaS content of inclusions in steel samples deformed at 1473 K was higher, while it was lower in the sample deformed at 1743 K. The CaO content changed inversely. Inclusions in steel samples deformed at 1473 K were a little harder than those in steel samples deformed at 1743 K due to the thicker CaS shell formed in the outer layer. The composition transformation of inclusions was mainly caused by the change of the thermodynamic equilibrium between steel matrix and inclusions at various temperatures. In solid steel at 1473 K, the strain concentrated on the soft calcium aluminate phase, resulting in higher deformation amount of inclusions. In semi-solid steel at 1743 K, the soft steel matrix deformed more than inclusions, leading in turn to a smaller deformation of inclusions.

Keywords:

Reduction, semi-solid steel, inclusion deformation, inclusion transformation, pipeline steel

1. Introduction

Inclusion deformation during the rolling process is essential for quality control of rolled products of pipeline steels. The impact factors of inclusion deformation can be divided into two categories. The first one is the properties of inclusions. Baker[1] obtained the relationship between relative plasticity and hardness of inclusions through the harness measurement of inclusion and matrix at different temperatures for a number of real and artificial inclusion systems. It was found that the relative plasticity of inclusion was related to the ratio of inclusion hardness to steel hardness. It was reported that Young's modulus exhibited a good linear correlation with Vickers hardness at low temperature, which was used to evaluate the low-temperature deformability of inclusions[2-4]. However, there was no relationship between high-temperature deformation and low-temperature Young's modulus of inclusions. Another key factor of inclusion deformation is the property of steel matrix. Many studies focused on the recrystallization behavior, crack formation and mechanical properties of solid steel during rolling process[5-7]. However, behaviors of steel in the semi-solid state at the temperature higher than conventional rolling temperature would be quite different but studied seldomly. Since Spencer's pioneering work in 1971[8], semi-solid processing of metals and alloys was studied mainly on behaviors and phenomena such as microstructure evolution and segregation formation[9, 10]. The technique has not been used in commercial production of steel. Soft and heavy reduction technologies were performed to casting steels with a liquid core in the purpose of eliminating defects such as center segregation and porosity[11-13]. But the soft reduction amount was limited by the formation of internal cracks[14]. Heavy reduction technology was applied at the end location of solidification stage with high solid fraction of 0.8-1.0[15, 16]. Difficulties in sampling from steel production and limitation of heating temperature endured by

experimental furnace impeded the studies on soft and heavy reduction technologies[15]. Moreover, the preoccupation of these studies has never been inclusions. Though inclusion transformation during solidification and cooling process of steels were widely studied[17-20], the effect of semi-solid state at high temperature on inclusion transformation and deformation was rarely reported. In the current study, inclusion deformation during the plain strain compression of solid steel and semi-solid steel was studied using Gleeble HDS-V40 CC-DR and semi-solid simulator. The effect of compression reduction on inclusion deformation was discussed.

2. Methodology

Steel samples were cut from a slab of pipeline steels with main compositions listed in **Table 1**. A Gleeble HDS-V40 thermomechanical simulator was used for direct resistance heating and plain strain deformation trials. Six tests were carried out in a vacuum of 5 x10^{-3} mbar. Thermocouples were connected to the surface of each steel sample at the midpoint of length. Steel samples with the size of 160 mm x 10 mm x 25 mm were clamped and water cooled at both ends, while the center part was heated to the target temperature under the control of thermocouple. The layout is shown in **Figure 1**.

Table 1 Main compositions of steel (wt %)

C	Si	Mn	P	S	Al_s	Ca	Mg	T.O
0.073	0.18	1.48	0.0082	0.0014	0.021	0.0008	0.0003	0.0019

The experimental scheme is listed in **Table 2**. Samples were heated to target temperatures at the rate of 5 K/s, held for a certain time, compressed with set reduction, and cooled rapidly. When the target temperature was 1473 K, the soaking time was 120 s. The soaking time was reduced to only 1 s under the target temperature of 1743 K to avoid the leakage of liquid steel. The last sample was heated without reduction to verify the formation of a semi-liquid zone in steel sample at 1743 K.

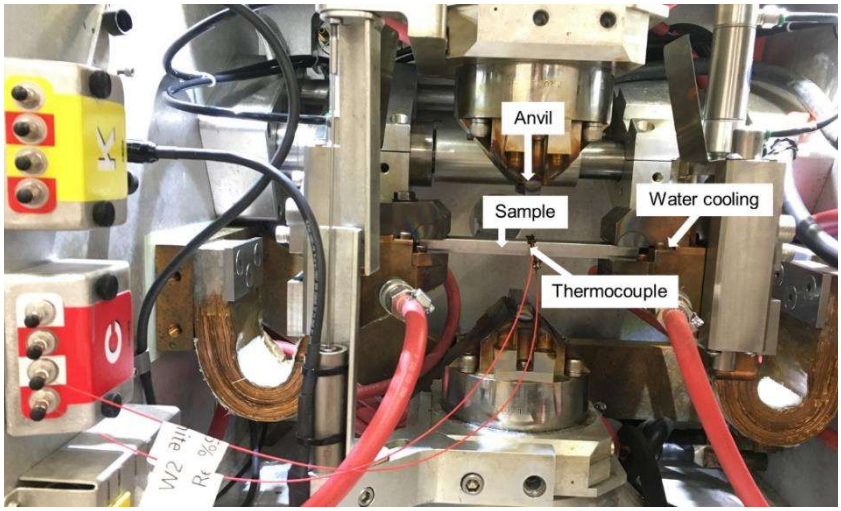

Figure 1 Device layout

Table 2 Experimental scheme

Sample	Temperature (K)	Holding time (s)	Reduction (%)	Strain rate (s^{-1})
A	1473	120	10%	5
B	1473	120	20%	5
C	1473	120	30%	5
D	1743	1	10%	5
E	1743	1	20%	5
F	1743	1	30%	5
G	1743	1	0%	-

Metallographic samples were cut from the center of samples after deformation, as shown in **Figure 2**. Automated scanning electron microscope was used for inclusion analysis, concentrating on the dash area, which was 3 mm in width. The accelerating voltage was 15 kV and the minimum size of detected inclusions was set as 2 μm. Another metallographic sample was cut from the original slab of pipeline steels as the baseline for the comparison of inclusion deformation.

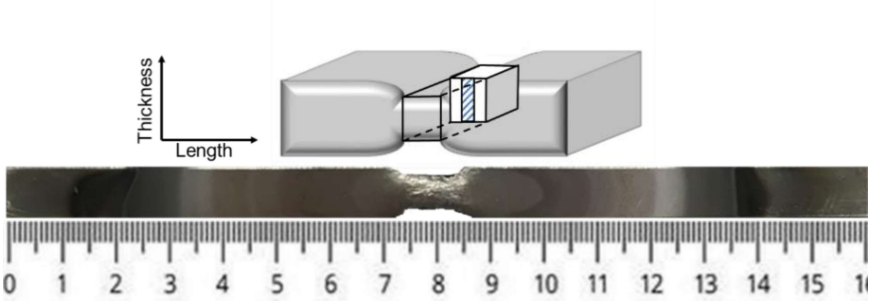

Figure 2 Sampling of metallographic sample

Liquidus and solidus of steel were calculated using FactSage 7.0. Thermodynamic calculation indicated that the solidus and liquidus of steel were 1730 K and 1796 K respectively. After plain strain deformation trials, the cross section at the midpoint of the sample, which was heated up to 1743 K without deformation, was prepared for metallographic analysis. Shrinkage cavities were observed from the center of the sample, as shown in **Figure 3**. It was inferred that there was a semi-solid zone formed in the center of samples heated up to 1743 K, while steel sample at 1473 K was pure solid. It should be noticed that the actual temperature in the center of the sample was a little bit higher than that detected by the thermocouple, which was connected to the sample surface.

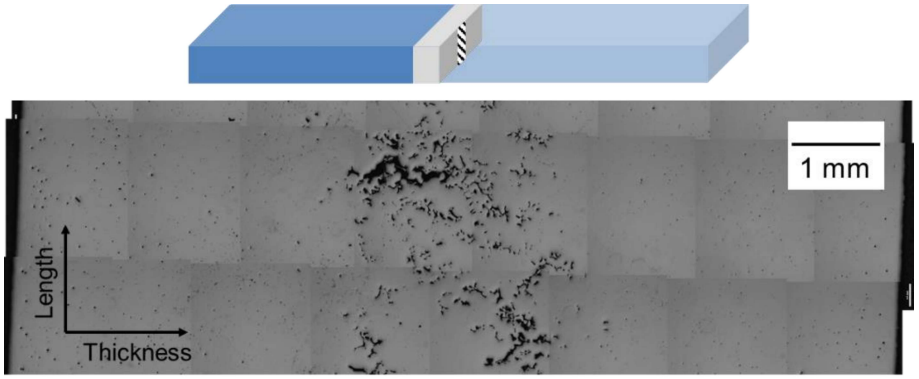

Figure 3 Shrinkage cavities in the center of steel sample heated up to 1743 K without deformation

3. Inclusion deformation in solid and semi-solid steel

Figure 4 shows the elemental mapping of a typical inclusion in original slabs. The average composition of inclusions in slabs was 60.41%Al_2O_3-17.49%CaO-10.77%MgO-11.33%CaS. The inclusion contained a Al_2O_3-MgO-rich core and a Al_2O_3-CaO-CaS outer layer. Inclusions were near-spherical before deformation with an average aspect ratio of 1.23. The aspect ratio of inclusions was the ratio of the maximum to minimum diameter of inclusions.

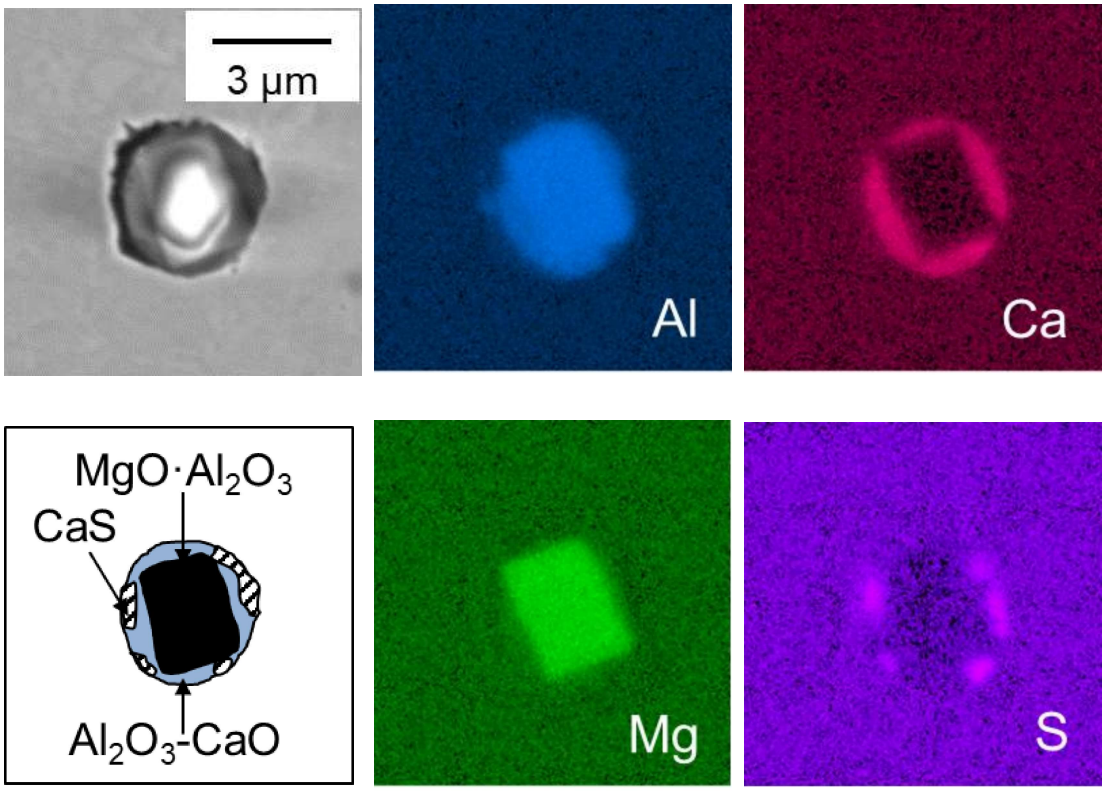

Figure 4 Elemental mapping of inclusions in original slab

The aspect ratio distribution of inclusions in steel samples deformed at 1473 K and 1743 K is shown in **Figures 5** and **6**. Each dot represented an inclusion particle. The aspect ratio of each inclusion was denoted by dot size. There was no obvious difference along thickness or width of each sample. The size of dot in **Figure 5** was larger than that in **Figure 6**, indicating a larger deformation of inclusions at 1473 K than 1743 K.

Figure 7 shows the average aspect ratio of inclusions in samples deformed at various temperatures and reductions. The average aspect ratio of inclusions increased from 1.23 in the original slab to 2.07, 2.23 and 2.30 in steel samples deformed at 1473 K with the reduction of 10%, 20%, and 30%. The corresponding average aspect ratios of inclusions were 1.26, 1.27 and 1.29 in steel samples deformed at 1743 K. The aspect ratio of inclusions increased with reduction in the solid steel, while it changed little in the semi-solid steel during the compression process.

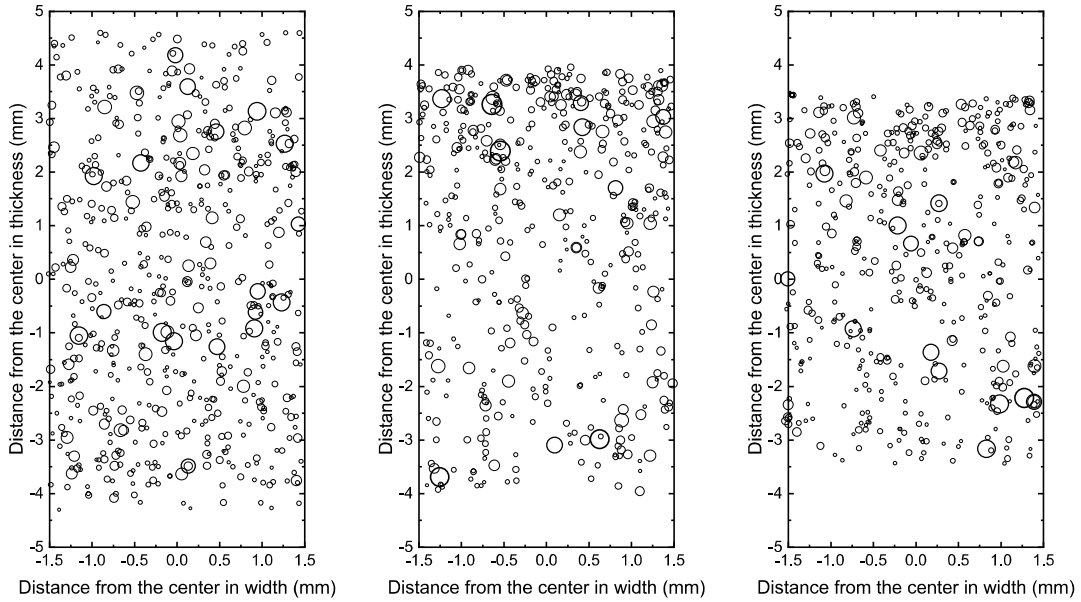

(a) (b) (c)

Figure 5 Aspect ratio distribution of inclusions in steel samples deformed at 1473 K with the reduction of (a) 10%, (b) 20%, and (c) 30%

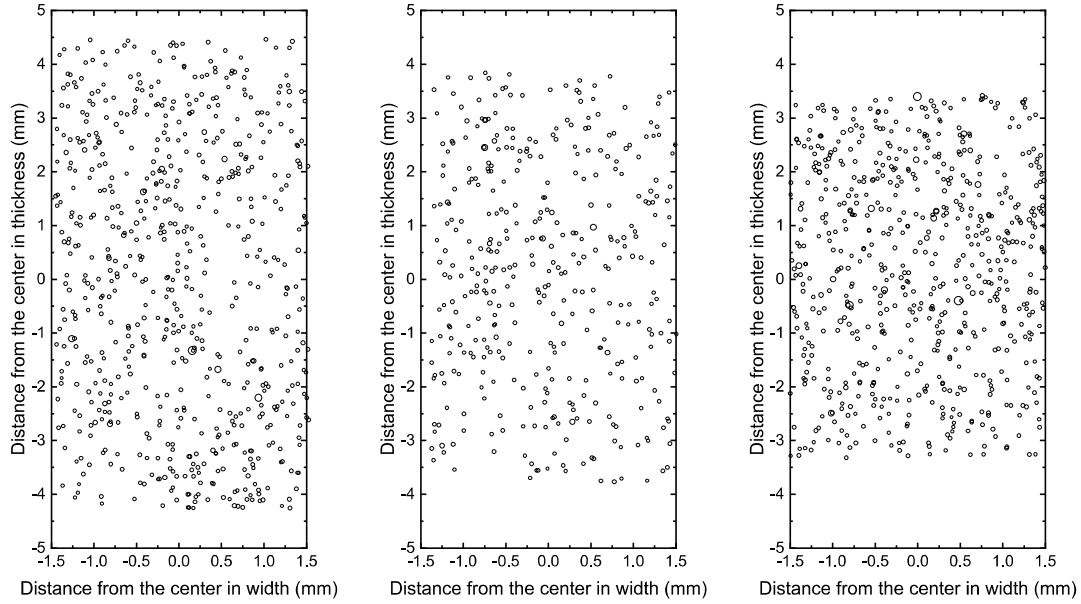

(a) (b) (c)

Figure 6 Aspect ratio distribution of inclusions in steel samples deformed at 1743 K with the reduction of (a) 10%, (b) 20%, and (c) 30%

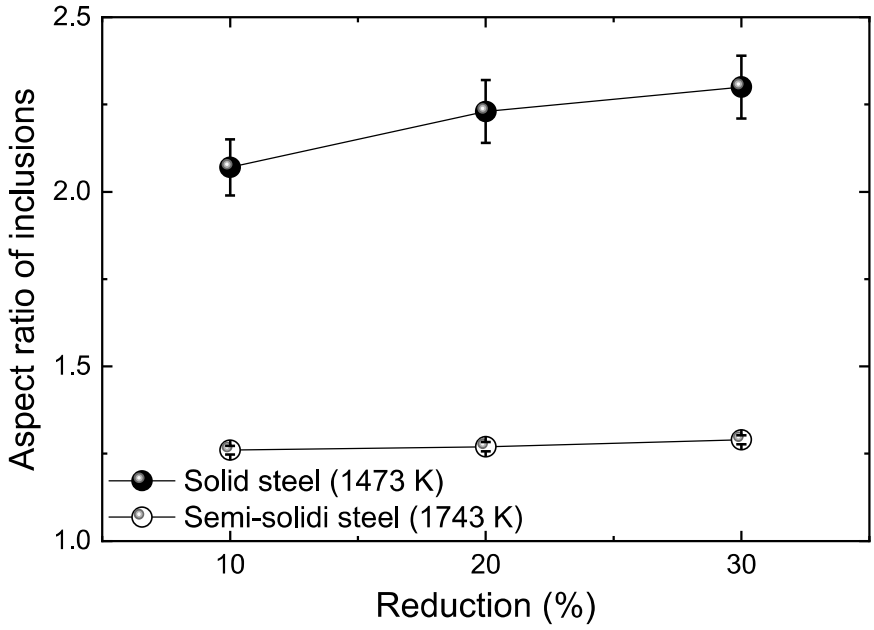

Figure 7 Variation of aspect ratio of inclusions with compression temperature and reduction

4. Composition of inclusions

Inclusions in steel samples deformed at 1473 K were plotted in CaO-CaS-Al_2O_3-MgO phase diagrams as shown in **Figure 8**. Each dot represented an inclusion. If the CaS content of inclusion was higher than MgO content, it was plotted in the triangle of CaO-CaS-Al_2O_3, otherwise in the triangle of CaO-Al_2O_3-MgO. The average composition of inclusions in each sample was plotted as a star. The average compositions of inclusions in steel samples deformed at 1473 K with different reduction were similar. It was 61.43%Al_2O_3-13.38%CaO-12.34%MgO-12.85%CaS under the reduction of 10%. When reduction increased to 20% and 30%, the average inclusion compositions were 60.59%Al_2O_3-13.03%CaO-12.74%MgO-13.69%CaS and 62.73%Al_2O_3-6.96%CaO-12.64%MgO-17.67%CaS, respectively. Compared to the average inclusion composition in the original slab, the CaO content of inclusions in steel sample deformed at 1473 K decreased about 6%, while the CaS content changed inversely. It indicated the transformation of inclusions from CaO to CaS occurred in the solid steel during the

heating process.

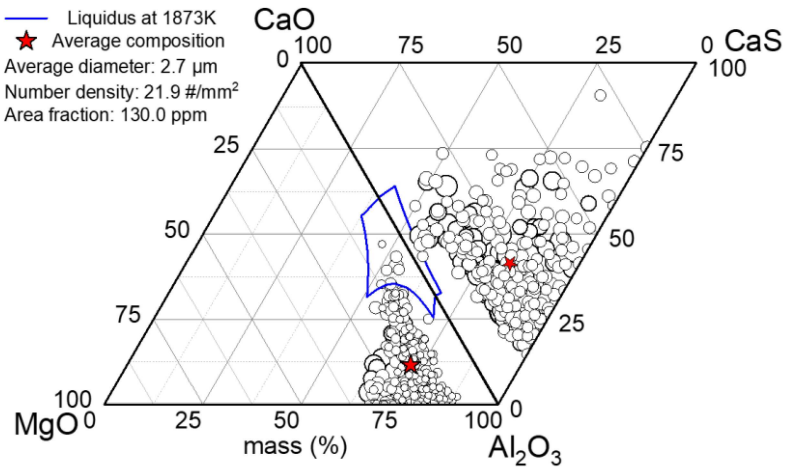

(a)

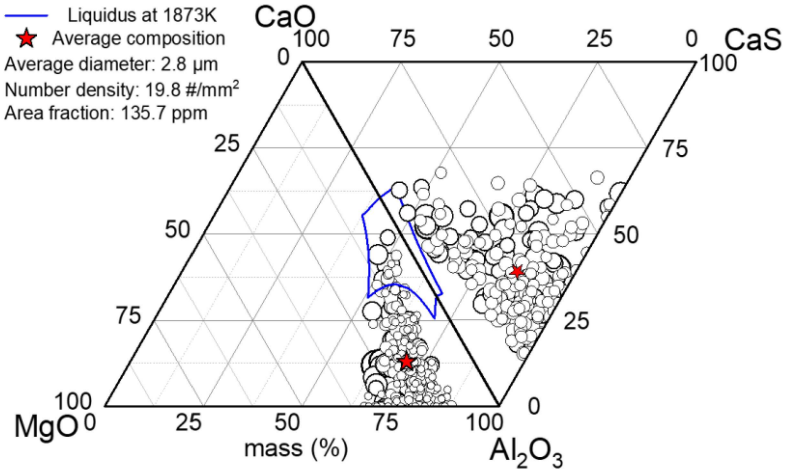

(b)

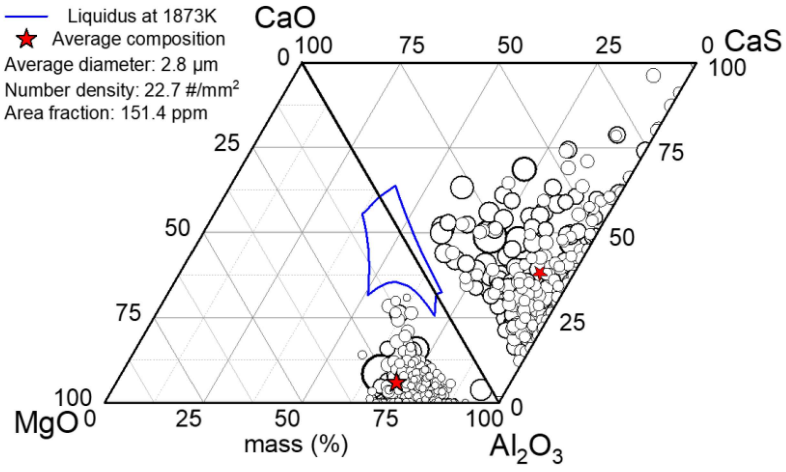

(c)

Figure 8 Distribution of inclusion composition in steel samples deformed at 1473 K with the reduction of (a) 10%, (b) 20%, and (c) 30%

Figure 9 shows the elemental mapping of typical inclusions in steel samples deformed at 1473 K. There were $MgO \cdot Al_2O_3$ phase, Al_2O_3-CaO-MgO phase, and CaS outer layer in inclusions. The amount of CaS layer in **Figure 9** was slightly higher than that in **Figure 4**, which was consistent to the transformation of inclusions from CaO to CaS. Inclusions were elongated during the plain strain deformation at 1473 K. The shape of inclusions changed from near-spherical before deformation to ellipsoid with the long axis along the direction of sample length.

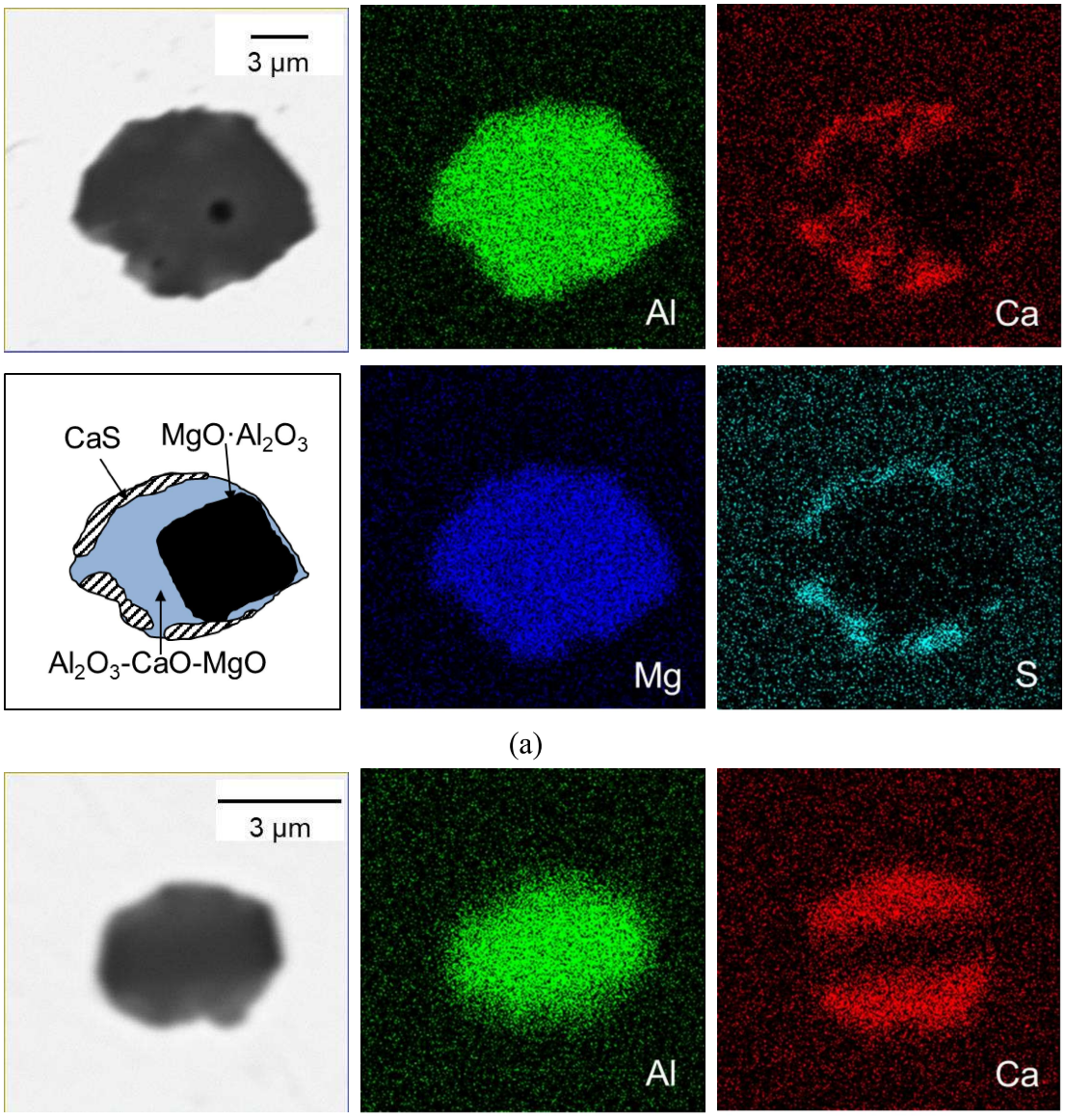

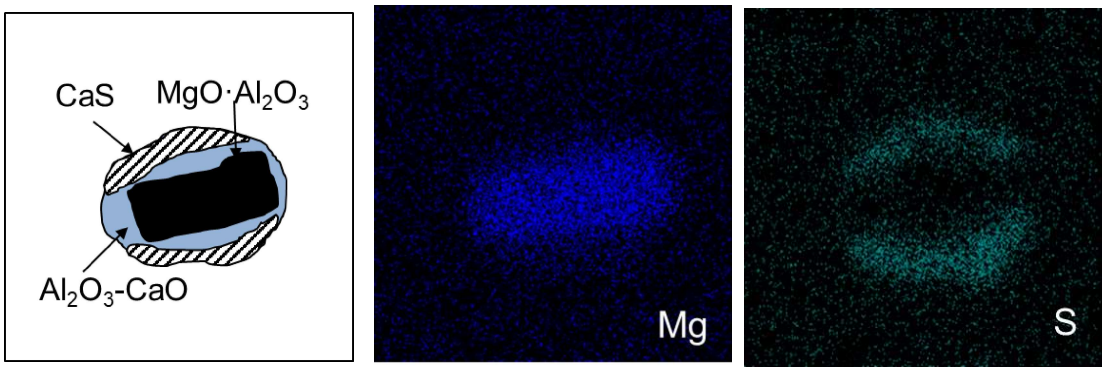

(b)

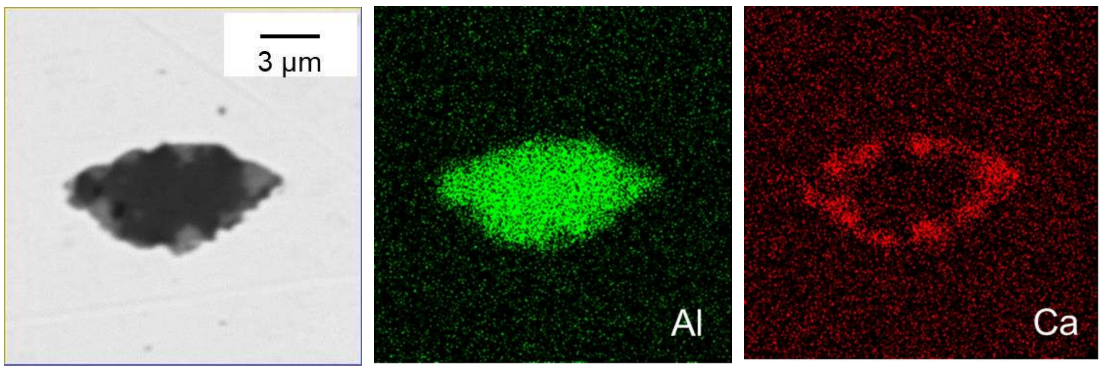

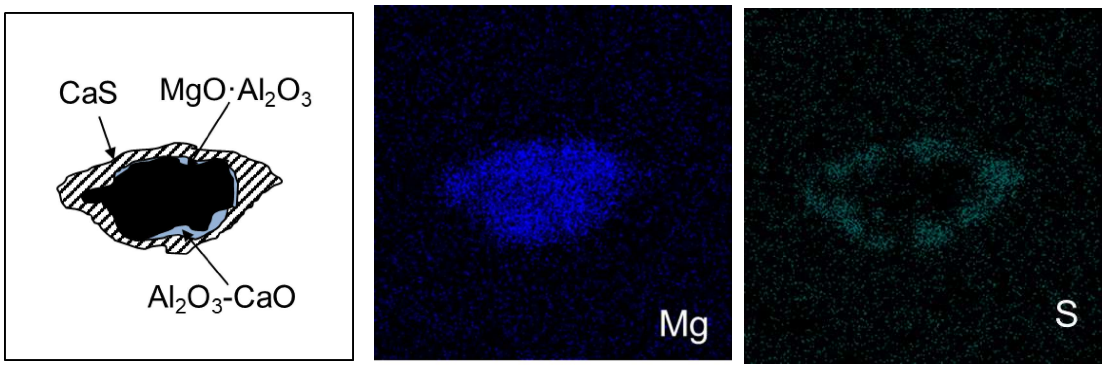

(c)

Figure 9 Morphology and elemental mapping of inclusions in steel samples deformed at 1473 K with the reduction of (a) 10%, (b) 20%, and (c) 30%

The composition of inclusions deformed in the semi-solid steel with a surface temperature of 1743 K was different from that in steel deformed at 1473 K. **Figure 10** shows the distribution of inclusion composition in steel samples deformed at 1743 K. The red star moved towards the low melting point area in the CaO-CaS-Al2O3-MgO phase diagram. Average compositions of inclusions in steel samples with reduction of 10%, 20%, and 30% were 58.61%Al_2O_3-22.03%CaO-12.53%MgO-6.83%CaS, 59.31%Al_2O_3-20.12%CaO-12.60%MgO-7.97%CaS, and 58.63%Al_2O_3-20.69%CaO-

11.14%MgO-9.64%CaS, respectively. The CaO contents of inclusions in steel samples deformed at 1743 K were about 3% and 10% higher than those in the original slab and steel samples deformed at 1473 K. The CaS content changed inversely by about 3% and 7% correspondingly. The transformation between CaO and CaS in inclusions in the semi-solid steel at 1743 K was contrary to that in the solid steel at 1473 K.

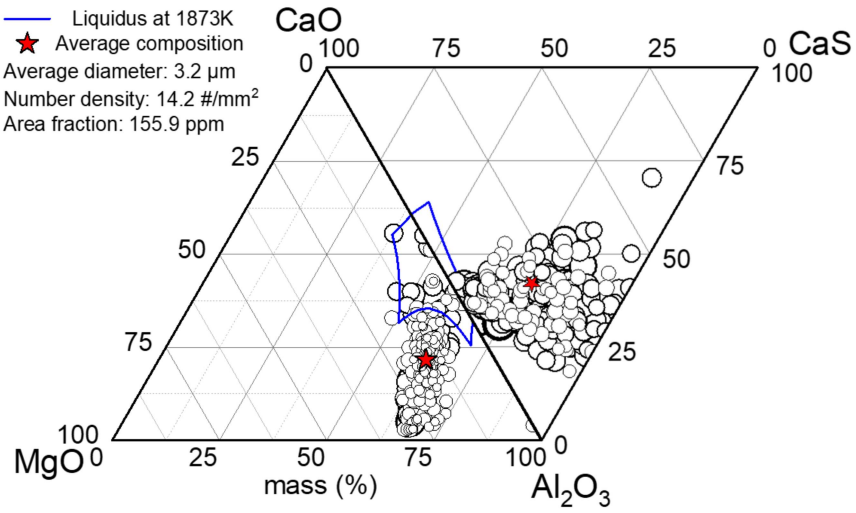

(a)

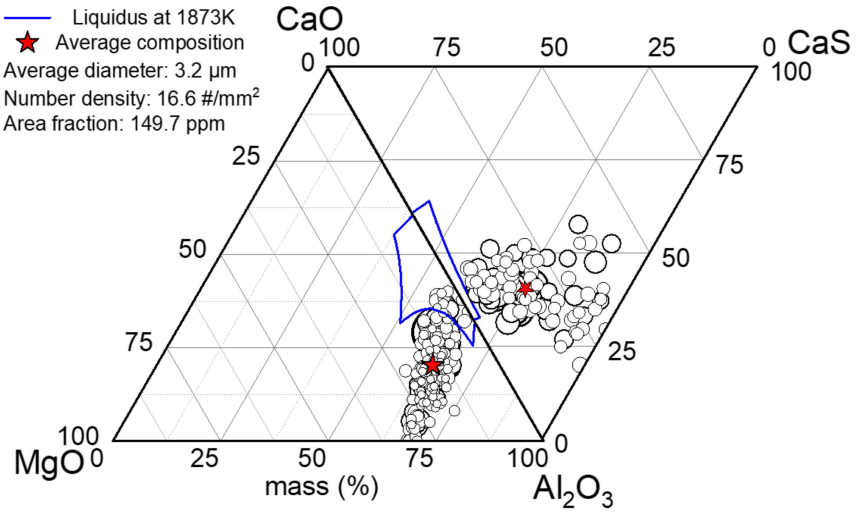

(b)

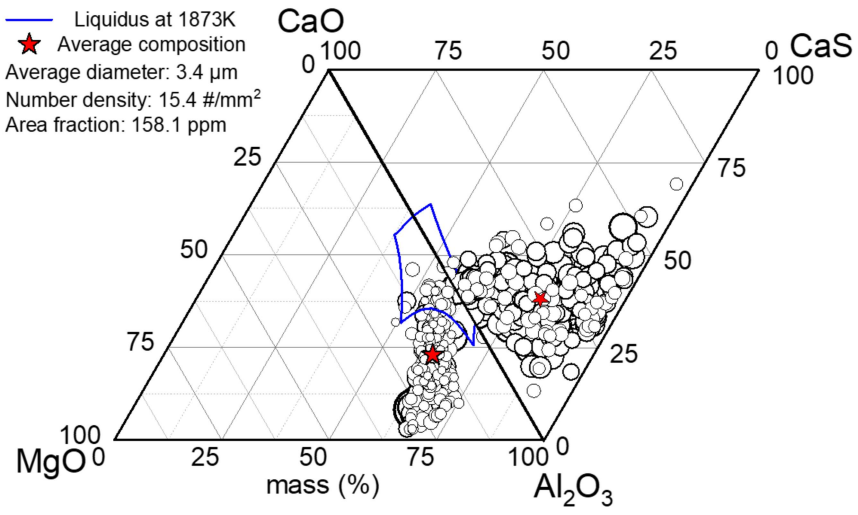

(c)

Figure 10 Distribution of inclusion composition in steel samples deformed at 1743 K with the reduction of (a) 10%, (b) 20%, and (c) 30%

The elemental mapping of typical inclusions in steel samples deformed at 1743 K was shown in **Figure 11**. Phases in inclusions were the same as that in inclusions in steel sample before deformation and deformed at 1473 K. While the amount of CaS outer layer slightly decreased. After deformation of the semi-solid steel matrix under the reduction of 10%, 20%, and 30%, inclusions were still near-spherical.

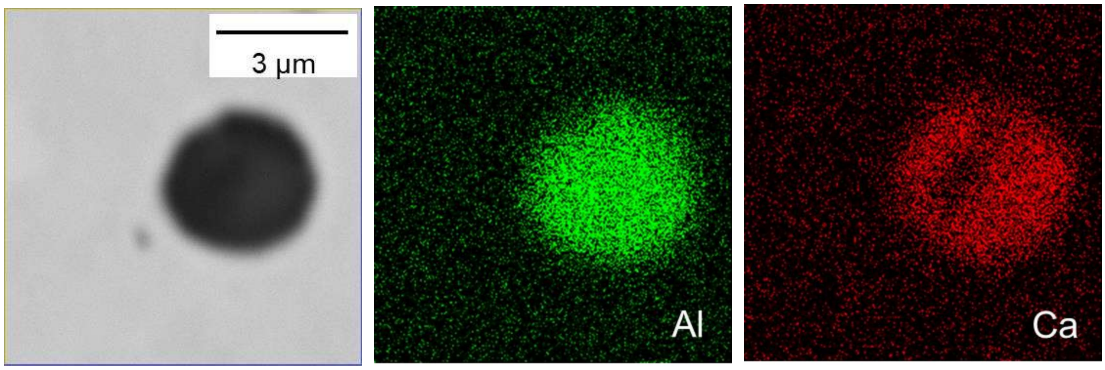

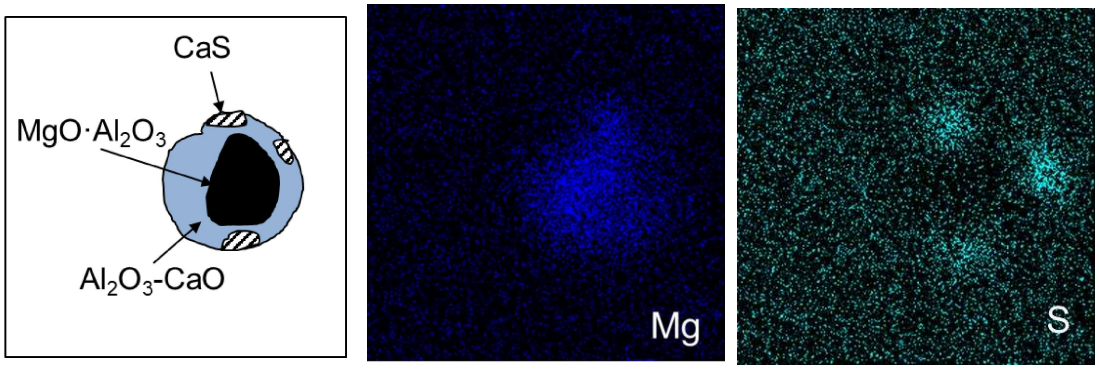
CaS
MgO·Al2O3
Al2O3-CaO
Mg
S

(a)

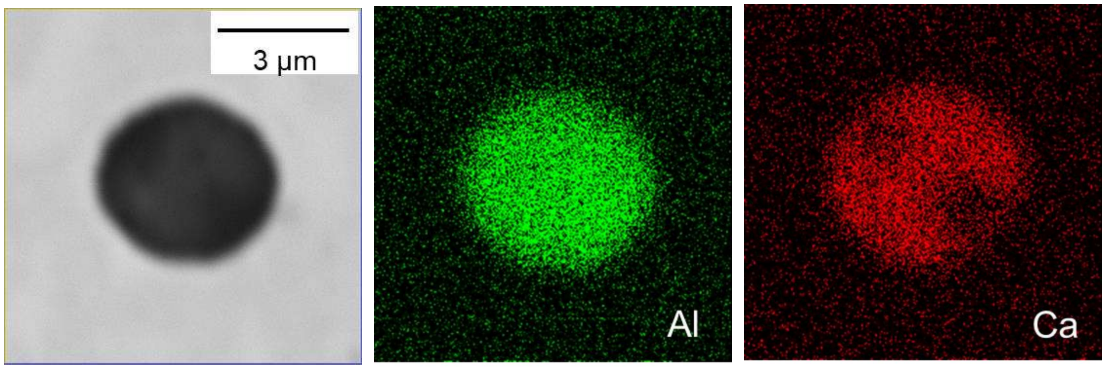
3 μm
Al
Ca

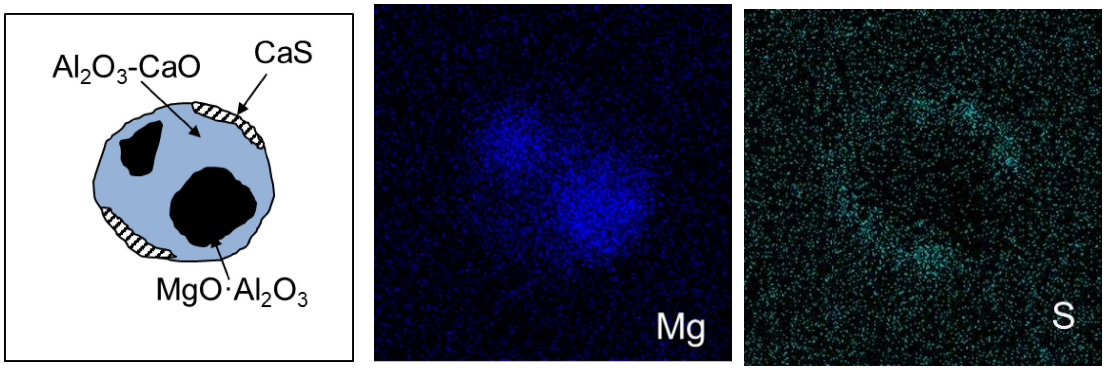
Al2O3-CaO
CaS
MgO·Al2O3
Mg
S

(b)

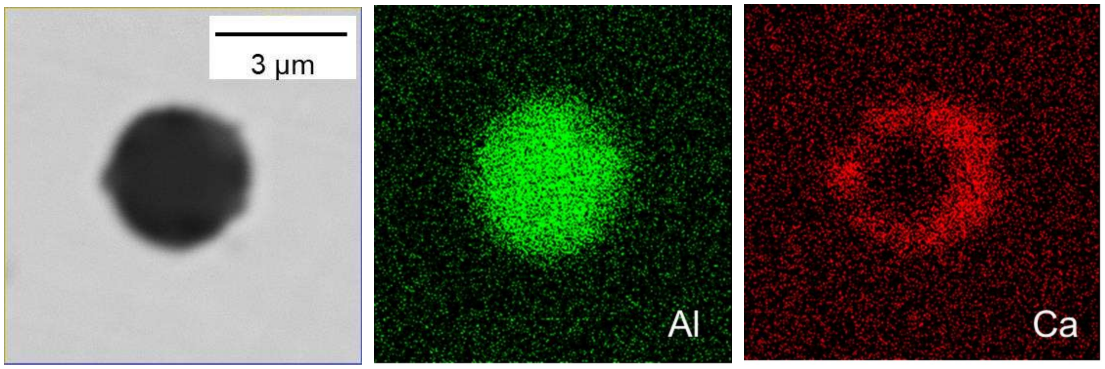
3 μm
Al
Ca

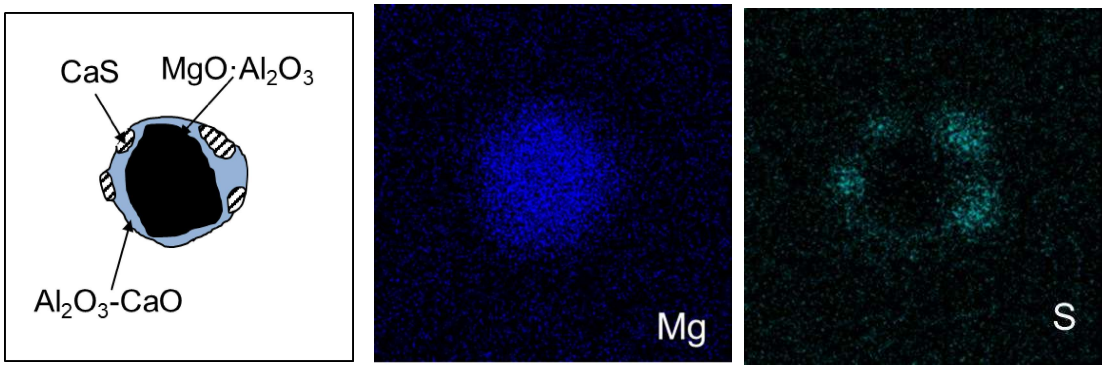

(c)

Figure 11 Morphology and elemental mapping of inclusions in steel samples deformed at 1743 K with the reduction of (a) 10%, (b) 20%, and (c) 30%

5. Thermodynamics of inclusion transformation

The inclusion transformation during solidification and cooling processes of steel was calculated by FactSage 7.0 with databases of FactPS, FToxid, and FSstel, as shown in **Figures 12**. Inclusions were liquid calcium aluminate and solid spinel in the molten steel. The liquid phase transformed into solid phases of $CaO{\cdot}2Al_2O_3$, $MgO{\cdot}Al_2O_3$, and CaS in semi-solid steel. The phase of $CaO{\cdot}2MgO{\cdot}8Al_2O_3$ precipitated with the further decrease of temperature, along with the decrease of $MgO{\cdot}Al_2O_3$ phase and increase of CaS phase. Inclusions changed from Al_2O_3-CaO-MgO to Al_2O_3-CaS-MgO-CaO through the whole solidification and cooling processes. The equilibrium compositions of inclusions at 1473 K and 1743 K were 65.06%Al_2O_3-3.80%CaO-9.22%MgO-21.91%CaS, and 64.91%Al_2O_3-10.97%CaO-9.78%MgO-14.33%CaS, respectively. The calculated values were quite different from the detected inclusion compositions, since the equilibrium was hardly reached during the short soaking time at 1473 K and 1743 K. Another reason was from inaccuracy of detecting temperature. The temperature in the center of the steel sample was higher than the surface temperature detected by the thermocouple. As shown in **Figure 12**, in solid steel, the equilibrium composition of inclusions was nearly constant under 1704 K without consideration of MnS phase. However, in liquid or semi-solid steel, the equilibrium content of CaO increased with

higher temperature, while CaS content decreased and disappeared.

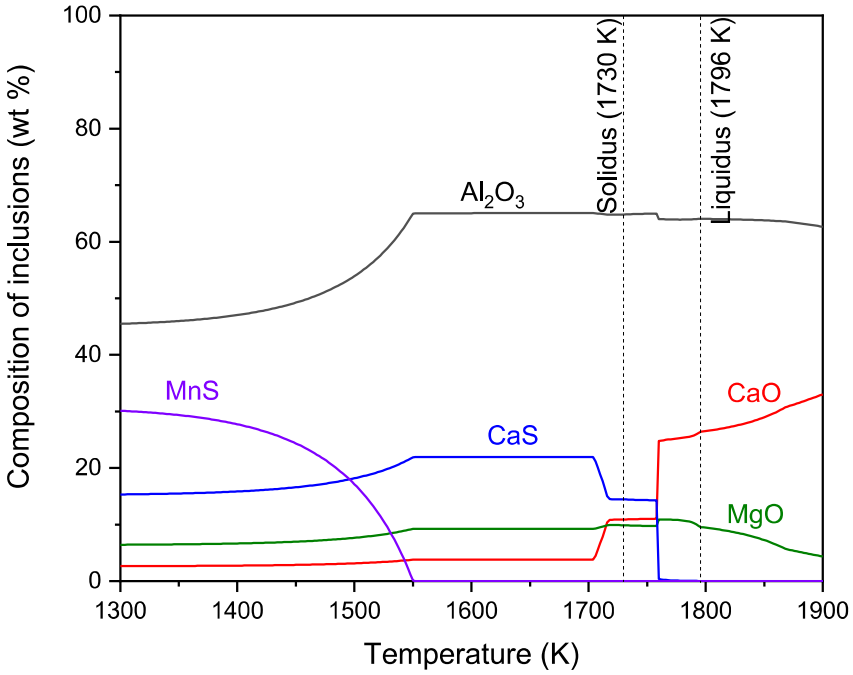

Figure 12 Inclusion transformation during solidification and cooling process of steel

6. Mechanism of inclusion deformation

The maximum stress obtained from the stress-strain curves of plain strain deformations was shown in **Figure 13**. It increased with reduction under the same temperature. For steel samples deformed at a certain temperature, reduction was a key factor affecting inclusion deformation, as the steel matrix and inclusions were similar. However, under the same reduction, the aspect ratio of inclusions after deformation was decided by the difference of hardness between inclusion phase and steel phase[1, 21]. For the hardness of steel matrix, **Figure 13** also showed that the maximum stress at 1743 K was significantly smaller than that at 1473 K under the same reduction, indicating a lower hardness of the semi-solid steel matrix at 1743 K than the solid steel matrix at 1473 K.

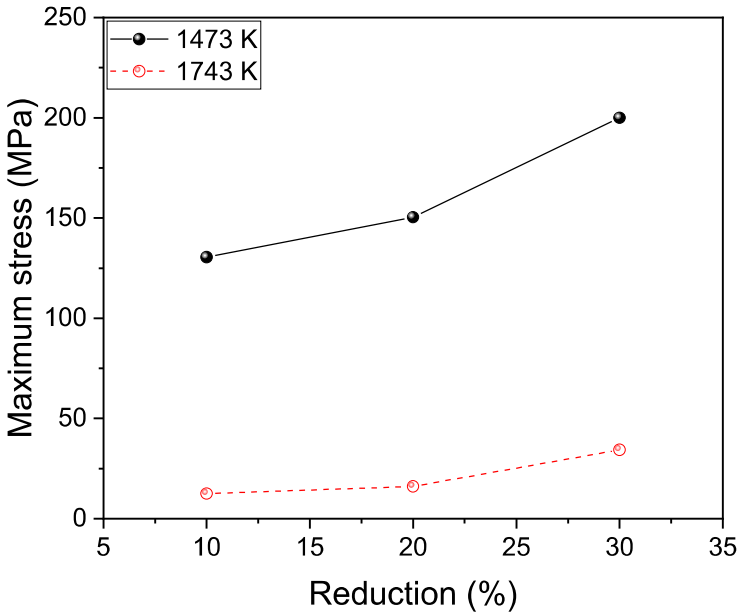

Figure 13 Variation of Maximum stress with reduction and temperature

The difference of inclusion deformation in solid steel at 1473 K and semi-solid steel at 1743 K is proposed in **Figure 14** by comparing the difference of hardness between inclusion phases and steel matrix. The sum strain of inclusion phase and steel matrix was represented by the shaded area in the lower part of **Figure 14**, which increased with reduction at the same temperature. The shaded areas were equal among samples deformed under the same condition of reduction. In terms of inclusions, phases of inclusions were $MgO \cdot Al_2O_3$, Al_2O_3-CaO-MgO, and CaS in the original slab, as well as samples deformed at 1473 K and 1743 K. For each case, the content of spinel was nearly the same, while the content of CaS outer layer was various. The CaS layer in inclusions, with a melting temperature of 2673 K, was a hard shell wrapped around low melting point calcium aluminate and the hard spinel core. More stain concentrated on soft phase than hard phase[22]. Although inclusions in steel samples deformed at 1473 K were harder than those in steel samples deformed at 1743 K due to the thicker CaS shell. With consideration of the hardness of steel matrix, the hardness of semi-solid steel was much lower than solid steel. The smaller difference between soft inclusion phase and

soft steel matrix resulted in a lower aspect ratio of inclusions in semi-solid steels after deformation. In **Figure 14**, though shaded areas were equal, the dark area, which represented the strain on inclusions was larger in steel samples deformed at 1473 K.

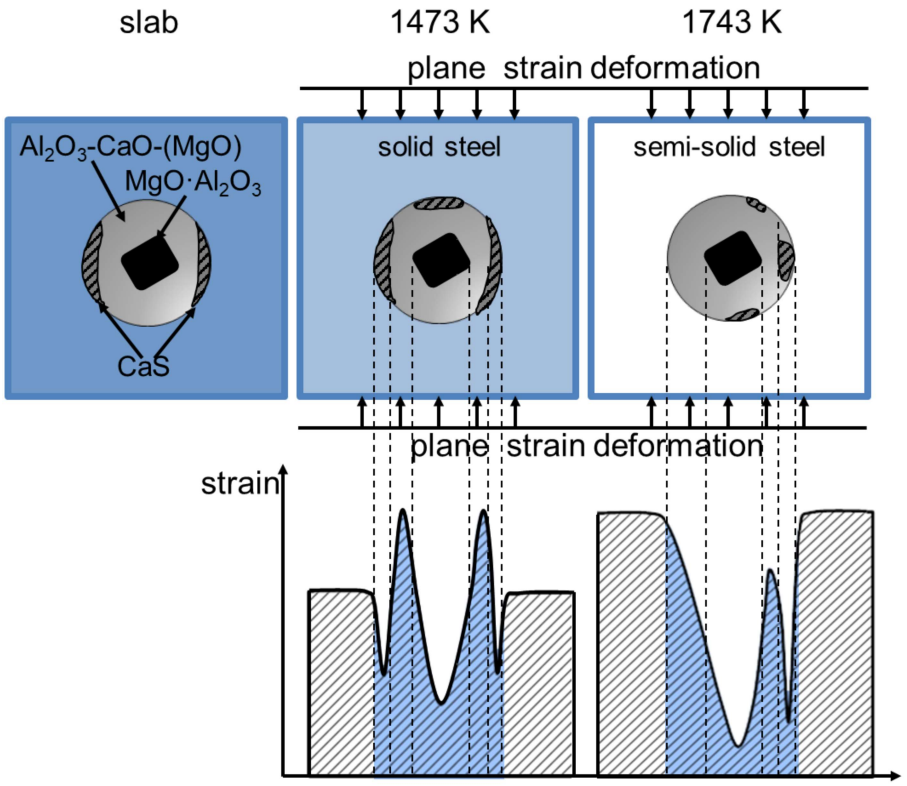

Figure 14 Deformation mechanism of inclusions in solid and semi-solid steel

7. Conclusions

In the current study, deformation of inclusions in both solid and semi-solid steel samples under various reductions was studied by experiments and thermodynamic analysis. Following conclusions were derived:

(1) A semi-solid zone was formed in the center of the steel sample heated up to 1743 K. Shrinkage cavities were observed. The maximum stress obtained from stress-strain curves of plain strain deformations indicated the semi-solid steel matrix at 1743 K was much softer than the solid steel matrix at 1473 K.

(2) The deformation of inclusions was much more in the solid steel deformed at 1473 K than that in the semi-solid steel deformed at 1743 K, when the reduction was

under 30%. In the solid steel deformed at 1473 K, the aspect ratio of inclusions increased with reduction, while the deformation of inclusions in the semi-solid steel changed little with reduction.

(3) The CaO in inclusions transformed into CaS in the solid steel at 1473 K, while the CaS content of inclusions in the semi-solid steel at 1743 K was lower than that in the original slab. Thermodynamic calculation showed that inclusions in steel samples deformed at 1473 K were harder than those in steel samples deformed at 1743 K due to the formation of a thicker CaS shell.

(4) In the semi-solid steel at 1743 K, less strain was concentrated on inclusions due to smaller hardness difference between the soft steel matrix and inclusions, resulting in a smaller deformation of inclusions during plain strain compression. Though there was a thicker CaS layer of inclusions in the solid steel at 1473 K, the amount of deformation was higher than that in the semi-solid steel at 1743 K due to bigger hardness difference between soft calcium aluminate in inclusions and hard steel matrix at 1473 K.

Acknowledgements

The authors are grateful for support from the National Natural Science Foundation of China (Grant No. U1860206, No. 51725402), the High Steel Center (HSC) at Yanshan University, and Beijing International Center of Advanced and Intelligent Manufacturing of High Quality Steel Materials (ICSM), and the High Quality Steel Consortium (HQSC) at University of Science and Technology Beijing (USTB), China.

References:

[1] T. Baker, K. Gave, J. Charles, Metals Technol. 1976, 3, 183.

[2] X. Jiang, J. Zhao, X Jiang, Comp. Mater. Sci. 2011, 50, 2287.

[3] L. Zhang, C. Guo, W. Yang, Y. Ren, H. Ling, Metall. Mater. Trans. B 2018, 49, 803.

[4] K. Wang, M. Jiang, X. Wang, W. Wan, Y. Wang, Metall. Mater. Trans. B 2020, 51, 95.

[5] L. Duprez, B. De Cooman, N. Akdut, Steel Res. Int. 2002, 73, 531.

[6] H. Yada, N. Matsuzu, Y. Matsumura, J. Tominaga, Tetsu-to-Hagane, 2009, 70, 2128.

[7] A. Pétein, P. Jacques, Steel Res. Int. 2004, 75, 724.

[8] D. Spencer, R. Mehrabian, M. Flemings, Metall. Trans. 1972, 3, 1925.

[9] M. Suery, M. Flemings, Metall. Trans. A 1982, 13, 1809.

[10] C. Chen, C. Tsao, Meter. Sci. Technol. 1999, 15, 981.

[11] J. Domitner, M. Wu, A. Kharicha, A. Ludwig, B. Kaufmann, J. Reiter, T. Schaden, Metall. Mater. Trans. A 2014, 45, 1415.

[12] C. Yim, J. Park, B. You, S. Yang, ISIJ Int. 1996, 36, S231.

[13] C. Ji, S. Luo, M. Zhu, ISIJ Int. 2014, 54, 504.

[14] R. Thome, K. Harste, ISIJ Int. 2006, 46, 1839.

[15] H. Li, T. Li, R. Li, M. Gong, Z. Wang, G. Wang, ISIJ Int. 2019, 59, 2283.

[16] J. Zhao, L. Liu, W. Wang, W. Zhou, H. Lu, Ironmak. Steelmak. 2019, 46, 227.

[17] S. Nurmi, S. Louhenkilpi, L. Holappa, Steel Res. Int. 2010, 80, 436.

[18] Y. Chu, W. Li, Y. Ren, L. Zhang, Metall. Mater. Trans. B 2019, 50, 2047.

[19] Y. Wang, W. Yang, L. Zhang, Steel Res. Int. 2019, 90, 1900027.

[20] W. Yang, C. Guo, C. Li, L. Zhang, Metall. Mater. Trans. B 2017, 48, 2267.

[21] K. Gove, J. Charles, Metals Technol. 1974, 1, 425.

[22] C. Elango, S. Yu, K. Naoya, M. Goro, F. Tadashi, Metall. Mater. Trans. A 2019, 50, 4111.

Captions:

Table 1 Main compositions of steel (wt %)

Table 2 Experimental scheme

Figure 1 Device layout

Figure 2 Sampling of metallographic sample

Figure 3 Shrinkage cavities in the center of steel sample heated up to 1743 K without deformation

Figure 4 Elemental mapping of inclusions in original slab

Figure 5 Aspect ratio distribution of inclusions in steel samples deformed at 1473 K with the reduction of (a) 10%, (b) 20%, and (c) 30%

Figure 6 Aspect ratio distribution of inclusions in steel samples deformed at 1743 K with the reduction of (a) 10%, (b) 20%, and (c) 30%

Figure 7 Variation of aspect ratio of inclusions with compression temperature and reduction

Figure 8 Distribution of inclusion composition in steel samples deformed at 1473 K with the reduction of (a) 10%, (b) 20%, and (c) 30%

Figure 9 Morphology and elemental mapping of inclusions in steel samples deformed at 1473 K with the reduction of (a) 10%, (b) 20%, and (c) 30%

Figure 10 Distribution of inclusion composition in steel samples deformed at 1743 K with the reduction of (a) 10%, (b) 20%, and (c) 30%

Figure 11 Morphology and elemental mapping of inclusions in steel samples deformed at 1743 K with the reduction of (a) 10%, (b) 20%, and (c) 30%

Figure 12 Inclusion transformation during solidification and cooling process of steel

Figure 13 Variation of Maximum stress with reduction and temperature

Figure 14 Deformation mechanism of inclusions in solid and semi-solid steel

Table 1 Main compositions of steel (wt %)

C	Si	Mn	P	S	Al_s	Ca	Mg	T.O
0.073	0.18	1.48	0.0082	0.0014	0.021	0.0008	0.0003	0.0019

Table 2 Experimental scheme

Sample	Temperature (K)	Holding time (s)	Reduction (%)	Strain rate (s^{-1})
A	1473	120	10%	5
B	1473	120	20%	5
C	1473	120	30%	5
D	1743	1	10%	5
E	1743	1	20%	5
F	1743	1	30%	5
G	1743	1	0%	-